IOP Conf. Series: Journal of Physics: Conf. Series **879** (2017) 012020 doi:10.1088/1742-6596/879/1/012020

Identifying potential disaster zones around the Verkhnekamskoye potash deposit (Russia) using advanced information technology (IT)

J J Royer[1], L O Filippov[1,2]

[1]Université de Lorraine, Laboaratoire GeoRessources, CNRS / CREGU, ENSG, 2 rue du Doyen marcel Roubault, BP F-54505 Vandœuvre-lès-Nancy, France.
[2]National University of science and technology MISIS, 4 Leninsky pr., 117049 Moscow, Russia

Email: jean.jacques.royer@gmail.com

Abstract. This work aims at improving the exploitation of the K, Mg, salts ore of the Verkhnekamskoye deposit using advanced information technology (IT) such as 3D geostatistical modeling techniques together with high performance flotation. It is expected to provide a more profitable exploitation of the actual deposit avoiding the formation of dramatic sinkholes by a better knowledge of the deposit. The GeoChron modelling method for sedimentary formations (Mallet, 2014) was used to improve the knowledge of the Verkhnekamskoye potash deposit, Perm region, Russia. After a short introduction on the modern theory of mathematical modelling applied to mineral resources exploitation and geology, new results are presented on the sedimentary architecture of the ore deposit. They enlighten the structural geology and the fault orientations, a key point for avoiding catastrophic water inflows recharging zone during exploitation. These results are important for avoiding catastrophic sinkholes during exploitation.

1. Introduction

Potassium is used in over 90% as fertilizers. This commodity is crucial for contemporary food industry. FAO[1] forecasts an increase by 70% to 80% of food demand in 2050 on expectations of increase in world population [1]. The efficient and responsible use of mineral fertilizers will play a vital role to meet the challenges of tomorrow's agriculture and future global demand for food [5]. World reserves of potash are reported in Table 1 showing that potassium resources are not regularly distributed worldwide. Canada, Belarus, and Russia have nearly 65% of all global reserves. Canadian deposits, the most important, are huge, thick, with high qualities and relatively easy to exploit. However, most of these lie at great depths (Saskatchewan > 900m; New Brunswick > 960m, Canada), and extraction costs tend to increase. They become difficult to exploit by traditional extractive methods, but technical solutions exist such as in-situ leaching (Solvay process) and could be an alternative where deposits are irregular in shape.

[1]Food and Agriculture Organization.

Table 1 – Production and potassium global resources (source: [21], [20])

Country	Mine Production[1]		Reserves	
	2014	2015[4]	Recoverable ore	K_2O Equivalent
Canada	11,000	11,000	4,200,000	1,000,000
Belarus	6,290	6,500	3,300,000	750,000
Russia	7,380	7,400	2,800,000	600,000
Jordan[3]	1,260	1,250	NA[2]	270,000
Israel[3]	1,770	1,800	NA	270,000
China	4,400	4,200	NA	210,000
Germany	3,000	3,000	NA	150,000
Chile	1,200	1,200	NA	150,000
United States	850	770	1,500,000	120,000
Other countries	50	50	250,000	90,000
United Kingdom	610	610	NA	70,000
Spain	715	700	NA	20,000
Brazil	311	311	300,000	13,000
World total (rounded)	38,800	38,800	NA	3,700,000

[1] Data are rounded to avoid disclosing company proprietary
[2] NA = Not available; [3] Total reserves in the Dead Sea are arbitrarily divided equally between Israel and Jordan; [4]Estimated.

Advanced 3D modelling can be very useful to estimate the recoverable resources by in-situ leaching and to anticipate future productions. The objectives of this study are to propose a model for studying the distribution of potash in ore deposits, and to infer areas at risk of surface collapses due to underground mining exploitation ([2], [3]).

2. The GeoChron theory

2.1. Introduction

The modern GeoChron approach tries to reproduce the sedimentary mechanisms which have led to the successions of the sedimentary formations [11]. One of the original ideas of GeoChron is to turn the complex 4D space-time into a simplified 3D one by mapping time on depth using a judicious choice of a curvilinear coordinate system. This model allows introducing *attributes* like *acceleration* or *sedimentary curvature* that can be directly connected to basin formation parameters such as *diffusion* or *advection sedimentation rate* [17]. It provides a framework for studying deformation in structural geology [13] and mineral resources potential study ([7], [4], [18]). It can be applied with benefit to the Verkhmekamskoye (Russia) potash deposits in order to better understand the sedimentary architecture of the geological formations.

2.2. What is GeoChron?

GeoChron is a mathematical model based on a transformation which relates the *present time Euclidean coordinates system* (in which geological observations are made), or Geological space (G-space), to a new depositional *time curvilinear coordinate system*, or Geo-Chronological space ($\overline{\text{G}}$-space). It can be seen as a time-stratigraphic model built in a depositional curvilinear coordinate system (u, v, t) superposed onto the geological present time coordinate system (x, y, z). The basic idea of the time stratigraphic model was initially suggested by [22] for 2D vertical cross-sections; the mathematical formulation of this concept was extended to the 3D space by [10].

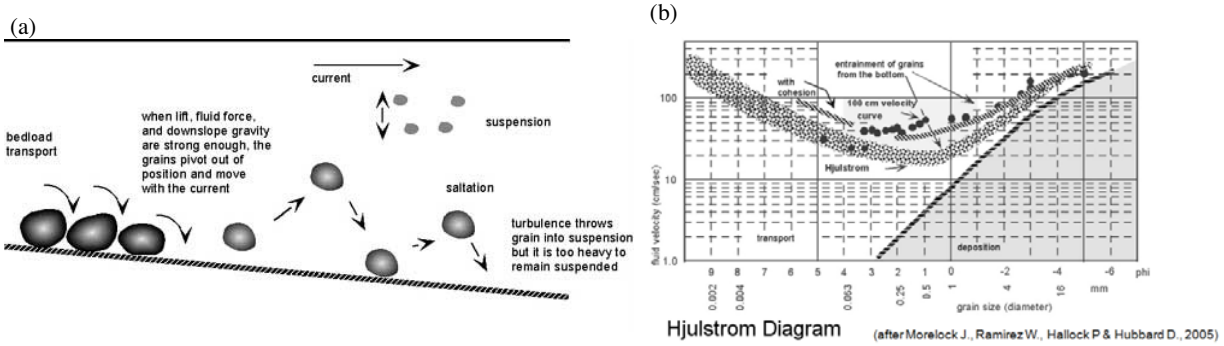

Figure 1. (a) Sediments transported under the combined effect of waves, currents, tides, gravity, rivers, evaporation, and tectonic subsidence. (b) Transport and deposition of sediments are functions of the grain size and the stream velocity or current velocity).

2.3. Intrinsic Sedimentary Attributes

Several attributes based on the lateral variation of the sedimentation rate can be introduced for characterizing the depositional environment, such as: (i) the *Einstein's curvature*, and (ii) the *sedimentary potential* ([11], p. 140). Some basic concepts are discussed: (i) the *vertical sedimentation rate* V_Φ corresponds to the amount of sediments (thickness) deposited per unit time ($m.s^{-1}$) defined by:

$$V_\Phi = \frac{1}{1-\Phi}\frac{1}{\|\boldsymbol{grad}\, t\|} \tag{1}$$

where t is time and Φ porosity. The sedimentation rate can vary or not laterally (Figure 1b). The sedimentation potential φ_ϕ is defined as the logarithm of the sedimentation rate $\varphi_\phi = \log V_\phi$.By definition, it is an *intrinsic*[2] property; (ii) the *lateral variation* of the sedimentation rate along the horizons (or sedimentary acceleration $\boldsymbol{A}$) is the gradient of the sedimentary potential calculated along the horizons (or isochrones surface). It is defined by: $\boldsymbol{A} = \boldsymbol{grad}_H\, \varphi_\phi$. This is a vector tangent to the horizons. The reader can consult the book by [11] for further information on this subject.

2.4. Einstein's curvature

A result of the Riemannian geometry shows that the volume variation of an elementary infinitesimal sphere submitted to deformations is proportional to the Einstein's curvature κ_E, an intrinsic property of the space (independent of the chosen coordinate system). In GeoChron, κ_E characterizes the lateral variations of the sedimentation rate ([11]; [17]). It is defined by:

$$\kappa_E = (\Delta_H V_\Phi)/V_\Phi \tag{2}$$

where Δ_H is the Laplacian calculated along a depositional horizon. It characterizes the relative variation of the layer thicknesses along the horizon. Mallet ([11], p. 142) shows that the Einstein's curvature (or sedimentary expansion) is related to the sedimentary acceleration by:

$$\kappa_E = div(\boldsymbol{A}) + \|\boldsymbol{A}\|^2 \tag{3}$$

where *div* is the divergence operator, $\boldsymbol{A}$ the sedimentary acceleration, a vector field measuring the variation of the sedimentary rate along the depositional horizons. The sedimentary acceleration vector is: (i) *tangent* to the horizons; (ii) *null* for constant sedimentation rate in the vicinity of the study location; (iii) oriented along the *increasing* layer thickness directions; (iv) the larger the module of the acceleration, the faster layer thickens in the direction of $\boldsymbol{A}$.

[2] e.g. independent on the coordinate system.

2.5. Sedimentary Models

Sedimentary basins result from the transportation of fluvial and/or marine sediment through waves, currents, gravity, tidal effects, rivers input, subsidence and tectonic events [12]. Models describing the redistribution of fluvial sediments during the formation of basins or the time-dependent evolution of landforms are usually based on two fundamental equations: (i) the *conservation* of sediments (continuity or mass balance) and (ii) the *sediment flux* evolution as a function of waves, currents, and gravity [6]. In the literature the conservation is written as (neglecting the porosity):

$$\partial_t Z = div\,(\boldsymbol{q}_s) + U \tag{4}$$

where $\partial_t Z$ is the derivative against time t, $div = [\partial u, \partial v]$ the 2D-divergence along the sedimentary horizon H, Z is the relative height of the column of sediment vertically stacked in the G-space (or equivalently, the relative altitude of the sea bottom counted from the sea level), $\boldsymbol{q}_s$ sedimentary flux, U accounts for combined effects of subsidence and compaction. Several models have been suggested for describing the sediment transport through the flux $\boldsymbol{q}_s$. One of the most used is the *diffusion-advection* model:

$$\partial_t Z = div(\boldsymbol{D}\,.\,\mathbf{grad}_H Z) + \boldsymbol{k}\,.\,\mathbf{grad}_H Z + U \tag{5}$$

where $\boldsymbol{D}$ is the diffusivity tensor (or dispersion) of sediments, $\boldsymbol{k}$ is the transport velocity of the sediments describing the advection term, the velocity is assumed to be conservative with null divergence ($div\ \boldsymbol{k} = 0$).

2.6. Sedimentary Models in GeoChron

The above classical approaches can be transposed directly into the GeoChron formalism noticing that the sedimentation rate plus the subsidence term $V_\phi + U$ can be expressed in function of the sedimentary rate according to ([11], p.35, Eq. 1.129; [17]):

$$\partial_t Z = V_\Phi + U = div\,\boldsymbol{q}_s + U \tag{6}$$

Deriving against time t, it comes (the subsidence term U is assumed to be global at the basin and time considered scales, it is locally constant by intervals, with a null derivative against time):

$$\partial_t V_\Phi = div\,(\partial_t \boldsymbol{q}_s) \tag{7}$$

where $\partial_t \boldsymbol{q}_s$ is the variation of the sedimentary flux as a function of time t at location (u, v), a quantity similar to the acceleration. If the flux is stationary, its derivative against time is null $\partial_t \boldsymbol{q}_s = \boldsymbol{0}$. This is not a realistic case as the sedimentary flux generally varies as a function of time (under Milankovitch cycles). Thus, the sedimentary acceleration $\partial_t V_\Phi$ captures the combined effects of the sedimentation, subsidence, compaction, loading and vertical uplifts of the basin as a function of time. Reporting Eq. (7) into Eq. (5) in the case of an isotropic diffusion coefficient d, it comes [17]:

$$(\partial_t V_\Phi) \,/\, (\Delta_H(V_\Phi)) = d + \boldsymbol{k}_d\,.\,(\boldsymbol{grad}\ V_\Phi)/(\Delta_H(V_\Phi)) \tag{8}$$

where d is the isotropic diffusion coefficient, $\boldsymbol{k}_d$ is the transport velocity of the sediments describing the advection term, Δ_H the Laplacian along the depositional surface. Introducing the sedimentary acceleration, Eq. (7) can be simplified into [17]:

$$\partial_t \ln V_\Phi = \kappa_E\, d + \boldsymbol{k}_d\,.\,\overline{\boldsymbol{A}} \tag{9}$$

where d is the isotropic diffusion coefficient, $\boldsymbol{k}_d$ is the transport velocity of the sediments describing advection term, $\overline{\boldsymbol{A}}$ the sedimentary acceleration, κ_E the Einstein's curvature.

2.7. Discussion

The time variation of the sedimentation rate $\partial_t \ln V_\Phi$ in eq. (9) is a relative dimensionless quantity that measures the vertical relative changes in the sedimentation rates V_Φ along isochrones of deposition in the geographical (or geological) space. The above relationship shows that this amount (which is easily calculated) is connected to the physical parameters describing the sedimentation (diffusion rate d,

Einstein's curvature $\varkappa_E$) plus an advection term described by a velocity $\boldsymbol{k}_d$ measuring the lateral sediment transport, multiplied by the acceleration vector $\overline{\boldsymbol{A}}$, a local measurement of the lateral variation of sediment rates along deposition surfaces. Several simple cases can be considered: (i) the sedimentation rate is *constant*, V_Φ = cst, the curvature $\varkappa_E = 0$ is null because the lateral variation of the

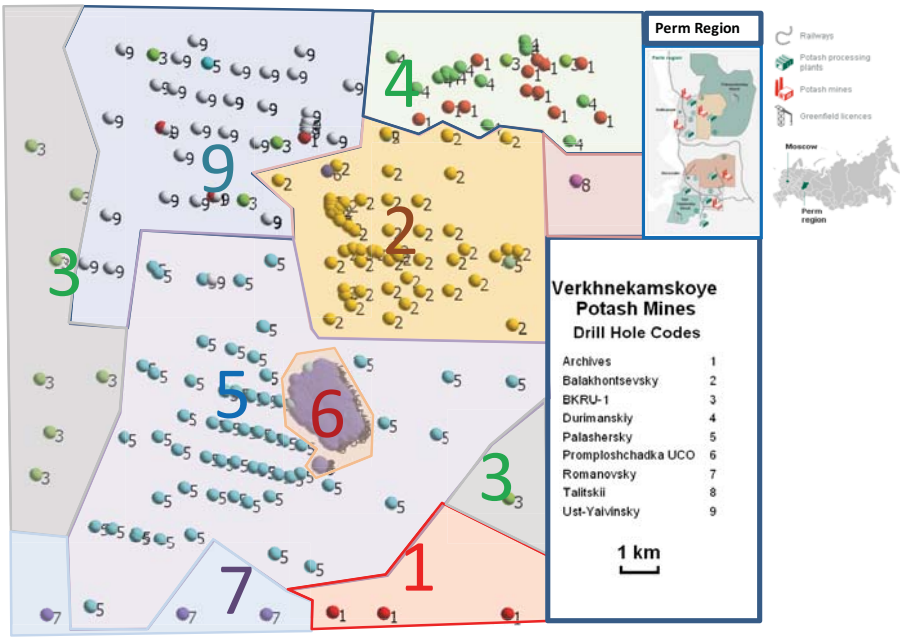

Figure 2. Drill location at Verkhnekamskoye deposit, Russia. Colors indicate type of ores.

sediment rate is zero, ***grad*** $V_\Phi = \boldsymbol{0}$, only vertical sediment inputs are accounted for (no lateral input); (ii) the sedimentation rate is an *harmonic* function, $\Delta_H (V_\Phi) = 0$, Eq. (9) simplifies into $\partial_t \ln V_\Phi = \boldsymbol{k}_d \,.\, \overline{\boldsymbol{A}}$ for which lateral sediment incomes due to the advection are taken into account; (iii) the general case (not an harmonic function) where diffusion and advection are considered. The above concepts has been developed and usually applied to clastic sediments; these concepts can also be extended to evaporitic sediments, the sediment rate being the proportion of precipitated minerals. This method has been applied to the case of the Verkhnekamskoye deposit.

3. Case study: the Verkhnekamskoye ore deposit

3.1. Geological settings

The Verkhnekamskoye deposit is a multi-layered fromation of potassium and potassium-magnesium salts; it is elongated along a North South (NS) direction and located within the Cherdynsky, Solikamsky and Usolsky districts of the Perm region, Ural, Russia. The NS extension of the deposit is about 140 km for a maximum width of about 42 km, making this 3,750 km^2 area, one of the biggest potassium salts producer in the World. Identified tectonic structures of sub EW strike, referred as the Durinsky and Borovitsky troughs, divide the sedimentary formation into three parts: the Northern, Central and Southern. The Verkhnekamskoye deposit is confined to the central part of the Solikamsk depression in the Predural edge trough. The Solikamsk depression, as part of the Predural trough, is bounded from the west by the Russian plate of the East European Platform, and from the east by the West Ural Folding Zone. Its western boundary is limited by the Krasnoufimsky deep fault, and the eastern one by the West Ural regional fault. The Palashersky and Balakhontsevsky areas host the Lower Permian halogen deposits made of saline rocks which contain potassium and potassium-magnesium formations, interbedded by terrigenous formations (lower sub-thickness of the salt-marl

layer), and on top, the over-salt layers comprising the upper sub-layer of the salt-marl, carbonate and various clastic layers. Quaternary deposits complete the stratigraphic section.

3.2. Methodology

Sedimentary attributes in §2 have been calculated on the Verkhnekamskoye deposit [9] using Gocad/SKUA scripts ([8], [14]) on a stratigraphic grid of 185×194×30 cells of size 100×100×2.5m

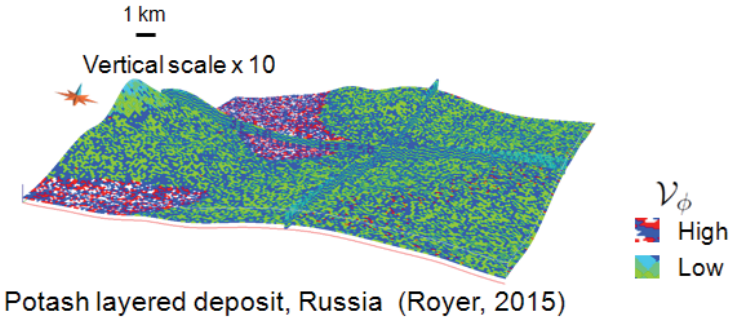

Figure 3. Sedimentation rate V_ϕ calculated on the stratigraphic grid. Highs (red) correspond to strong thicknesses with a high sedimentation rate V_ϕ , indicating the thickest layers [17].

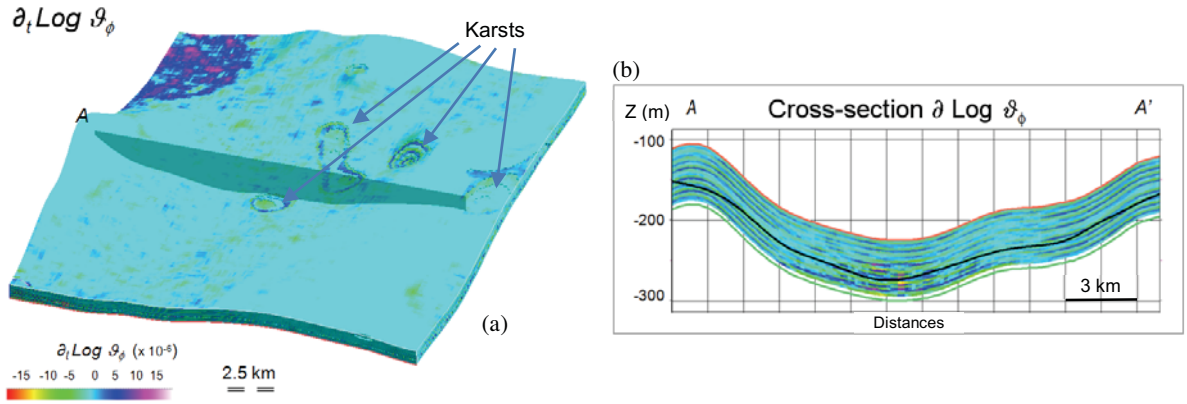

Figure 4. (a) Derivative against time of the potential (∂_t ln V_Φ), painted on an isochronous surface (left): the sedimentation rate (V_Φ) is almost constant everywhere along a layer, except in the upper left corner, and around the collapsed zones (karsts); (b) it varies however in function of the depositional time (or depth) as shown on the vertical cross-section (right), in particular at the center of the basin, and clearly delimits the sedimentary layers.

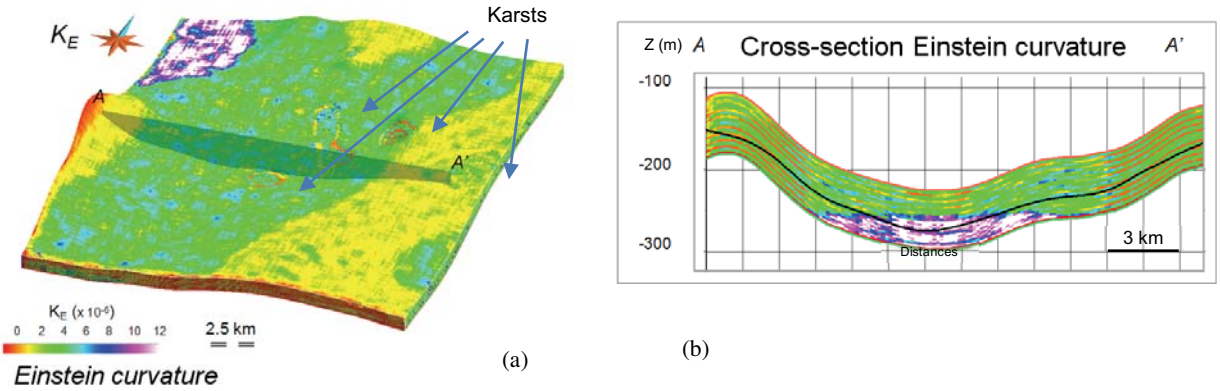

Figure 5. (a) The Einstein curvature emphasizes a NE oriented structure to the East of the studied area, and strong values in the NW upper left corner; (b) Vertical cross-section showing a strong change in curvature values in the middle of the basin.

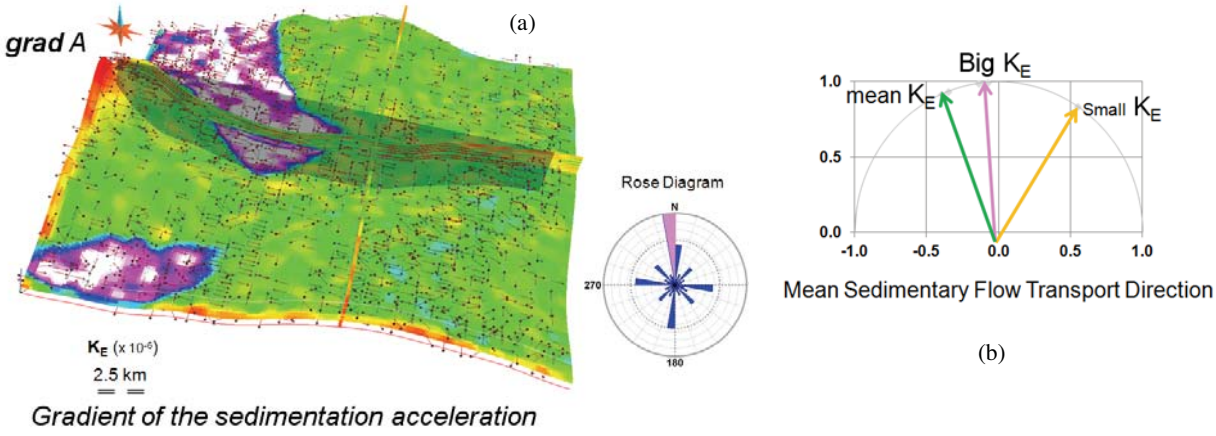

Figure 6. (a) Orientation statistical diagram (rose diagram, right) of the sedimentary acceleration gradient (arrows) (left) points out a main orientation along the NNW directions, with small contributions in EW and NS directions. These directions seem related to the main on-filling sedimentation supply directions during the formation of the basin; (b) Isotropic diffusion coefficient and velocity vector estimated by multi-variable linear regression on three classes of curvatures, strong (purple), medium (green) and small (yellow). Directions of infillings are given on the orientation diagram for each class.

(a total of more than one million (1,000,000) cells) of the 3D model built by [16] (Figure 2). The stratigraphic grid was adjusted between the top and the base of the mineralized zones to calculate sedimentary attributes along the geological layers (Figure 3).

3.3. Temporal variation of the sedimentation rate ∂_t ln V_ϕ

The variation over time of the sedimentation rate ∂_t ln V_Φ, a dimensionless relative quantity, measures the relative vertical variations on the sedimentation rate V_ϕ along the isochrones of deposition. It was calculated in 3D throughout the stratigraphic grid (Figure 4a). Represented in vertical section, it is often zero but sometimes varies brutally and emphasizes remarkably the mineralized boundary layers (Figure 4b). Painted on isochronous surfaces, this attribute is almost constant to zero everywhere along a sub-layer showing that the sedimentation rate is almost constant everywhere except in the NW left corner, and around the collapse zones (karsts). In the case of Verkhnekamskoye potash deposit, the derivative against time of the sedimentation rate ∂_t ln V_Φ is a sedimentary attribute well suited to identify potential karsts areas and water infiltration, and can help to define risk areas.

3.4. Einstein's Curvature

The Einstein's curvature κ_E characterizes the lateral variations of the sedimentation rate and is related to the sedimentary acceleration vector $\boldsymbol{A}$. It was calculated on the entire mineralized zone (Figure 5a, and Figure 6a). Along the layer, the Einstein's curvature structures the mineralized zone in three areas: (i) *strong* values (indicating strong variations in the sedimentation rate) in the NW corner at the same locations where the acceleration was variable; (ii) a *central* area with average values oriented NE with a NW branch at the top left of the map; (iii) a zone with *low* values close to zero on topographic highs and emphasizing a NE direction to the east of the map. The karsts in this area are clearly outlined as zero-curvature contours. Figure 6a represents the curvature of the deepest layers (KPIII) and shows strong variations in the NS corner of the study area. NE directions appear much less clear at depth. In vertical cross-sections (section AA ') (Figure 5a,), the κ_E curvature (i) highlights the limits of the mineralized layers, (ii) shows tenuous fluctuations along the layers showing that the rate of sedimentation is not constant as one can think reading the maps of the acceleration, (iii) identifies areas with high variation of the curvature at the bottom centre of the basin. Thus, the curvature κ_E, like the acceleration, can be used to identify the layers boundaries and areas with karsts risks. Its resolution is better than that of the acceleration to identify weak relative variations.

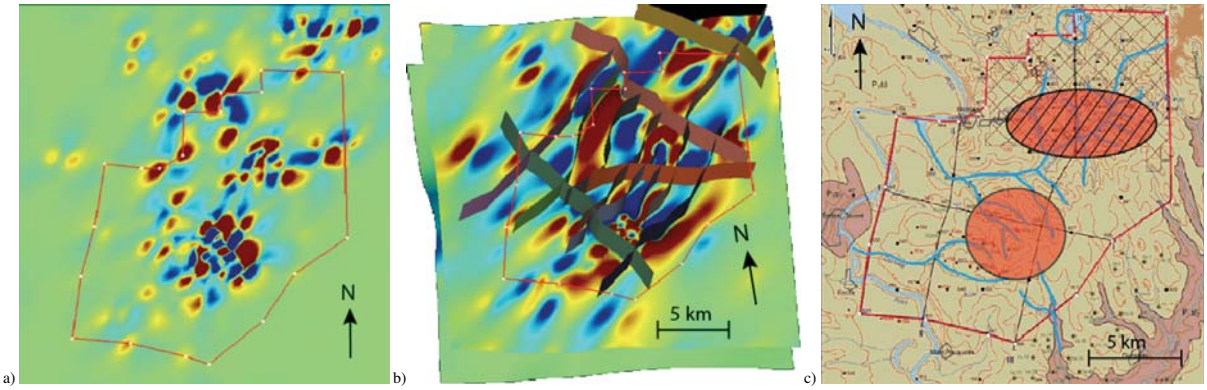

Figure 7. (a) Gaussian curvatures calculated on the topography for identifying faults; (b) Identified faulted structures extended at depth and reported on the mean curvatures map of the salt top layer showing a good fitting; (c) Surface map of the Verkhnekamskoye deposit (red line) with rivers and pools, and potential disaster zones (orange) identified as downward infiltrations of water along faulted zones which dissolve salts at depth.

3.5. Gradient sedimentary acceleration

The sedimentary gradient vector, or sedimentary acceleration, $\boldsymbol{A} = \boldsymbol{grad}\ V_\Phi$ was calculated at each point of the stratigraphic grid, and its orientation has been materialized as arrows along a stratigraphic horizon (Figure 6a). At first glance, the directions seem to be randomly distributed along the horizons. However, the directions diagram (rose graph) shows a preferential NNW orientation, with contribution from both conjugated directions EW and NS. These directions seem related to on-filling sediment supply directions.

3.6. Diffusion coefficient and transport velocity vector

The isotropic diffusion coefficients d and the transport velocity vector $\boldsymbol{k}_d$ defined by the formulation of Eq. (8) were estimated using multivariable linear regression on the three classes of curvatures, *strong* (purple), *medium* (green) and *small* (yellow) (Figure 6b) at the nodes of the stratigraphic grid over the study domain. The isotropic diffusion values d are relatively similar and vary between $0.67_{\pm.06}$ (high values) and $0.54_{\pm.02}$ (small to median values).

The transport velocity vector $\boldsymbol{k}_d$ and its direction change according to the curvature κ_E, and its module is in the same order of magnitude as those of the isotropic diffusion coefficient d; its orientation is given in the stereogram of Figure 6b for each of the classes. The direction of $\boldsymbol{k}_d$ is oriented towards NE for low curvature values, along the NNW direction for the mean values, and along NS for high values. The transport velocity vector materializes the direction and flux of the incoming sediment flow during sedimentation.

3.7. Identifying potential faults and disaster zones

In order to identify possible faulted lineaments [15], the Gaussian (κ_G) and mean (κ_H) curvatures maps have been calculated both on the topographic surface and at the top of the salts layers (Figure 7a & b). The lineaments identified on the topography map (Figure 7a) seem to extend at depth as shown by the curvature maps calculated on the top of each salt layers (Figure 7b); thus, they were interpreted as sub-vertical faults that cross-cut the mineralized salt layers. They are mainly oriented along a NE direction (N45), while their conjugates are approximately orthogonal along a NW one (N135). These two directions are visible on the rose diagram of Figure 6a, indicating that these faulted structures were originally active at the early stages during the basin in-filling, and are probably of deep crustal origin. These faults are weak structures that may open potential favorable drains for surface water infiltrations, provoking the dissolution of salts at depth, and therefore causing disaster at the surface by the development of sinkholes.

4. Conclusions

Several significant scientific results were obtained, both on the 3D modelling aspects of the Verkhnekamskoye potash deposit (Russia) and on the sedimentary characteristics of the deposit. The curvature of the horizon was used to define areas at risk of water invasion, and to establish a risk map. Several sedimentary attributes were calculated (sedimentation rate, acceleration, curvature, isotropic diffusion coefficient, sediment transport velocity). These parameters emphasize remarkably well the layers boundaries, the karsts areas, and the sedimentary architecture of formations with the main directions of the sediment income, the position of lineaments and fractures. However, several aspects remain to be explored. In particular, the role of water and hydrogeology in the deposit as a risk factor of liquid intrusion during the mining operation. This could be a research subject for the coming years. This study provides a 3D model of the mineralization of the Verkhnekamskoye region, which to our knowledge has never been done before.

5. Acknowledgements

The authors would like to express theirs thanks to the Lorraine Region for the financial support of Arcus Project and to the Gocad consortium.
The work was partially supported by the Government of Perm Krai, Russia (grant C-26-004-07).

References

[1] Alexandratos N, and Bruinsma J, 2012. World agriculture towards 2030/2050: the 2012 revision. ESA Working paper No. 12-03. Rome, FAO, 154p.
[2] Andrejchuk A. (2002) - Collapse above the World's largest potash mine (Ural, Russia). *Int. J. Speleol.*, **31** (1/4), 137-158
[3] Ashrafiantar N, Hebel H P and Busch W 2011. *Monitoring of mining induced land subsidence - Differential SAR interferometer and persistent interferometer using TerraSAR-XData in comparison with Envisa Data*. 4th TerraSAR-X Science Team Meeting, 14-16 Feb., DLR, Oberpfaffenhofen, Germany, 7p
[4] Camara N., Royer J.J. (2015) - 3D Modeling and Mineral Resources Estimation of the Kofi Birrimian Gold deposit, Zone C, Mali, 13th Biennial SGA meeting, Nancy, France, 1-4.
[5] FAO, 2008 : ftp://ftp.fao.org/docrep/fao/003/Y1997E/FRA%202000%20Main%20report.pdf
[6] Fagherazzi, S. and Overeem, I.(2007) - Models of Deltaic and Inner Continental Shelf Landform Evolution. *Annu. Rev. Earth Planet. Sci.*, **35**, 685-715.
[7] Fuentes L. (2012) – Characterizing and modeling phosphate rocks of the La Culebra area of the La Linda Los Bancos deposit (Venezuela) in order to evaluate phosphate resources. Msc University de Lorraine, ENSG, 94p.
[8] gOcad Research Group - http://www.gocad.org/w4/
[9] Kydryachov A I et al 2006. *Mineral and raw materials inventory of the Perm Region*, Perm, 464p.
[10] Mallet, J. L. (2004) – Space-Time Mathematical Framework for Sedimentary Geology. *Mathematical Geology*, **36**(1), 1-32.
[11] Mallet, J. L. (2014) – *Elements of Mathematical Sedimentary Geology: the GeoChron Model*. EAGE, European Ass, of Geoscientists & Engineers, ISBN 978-90-73834-81-1, 374p.
[12] Martinez, P. A. and Harbaugh, J. W. (1993) - *Simulating Nearshore Environments*. Computer Methods in the Geosciences, Vol. 12, Pergamon Press, Oxford.
[13] Mejia-Herrera P., Kakurina M., Royer J.J. (2015) Predictors for Off-fault Au Assessments from 3D Restoration – Mount Pleasant Area, Western Australia - 13th Biennial SGA meeting, Nancy, France, 1-4.
[14] Mira Geoscience - http://www.mirageoscience.com/
[15] Roberts A. (2001) – Curvature attributes and their application to 3D interpreted horizons. *First Break*, **19**(2), 85-100.
[16] Royer J.J. (2015a) - Développement des Connaissances Scientifiques en Flottation Hautes Performances

utilisées pour Exploiter les Ressources Minérales. Amélioration des Procédés d'Enrichissement du Minerai de la Mine de K-Mg de Verkhmekamskoye (Russie) - "Modélisation 3D et Optimisation de la Flottation". Programme de Coopération Scientifique avec l'Université d'État de Perm, Russie. Rapport interne, ENSG, UL, Nancy, 43p.

[17] Royer J.J. (2015b) - *Some GeoChron Unrevealed Sides: Linking the GeoChron Einstein Curvature with Classical Sedimentary Depositional Models* . 35th gOcad Meeting, Nancy, 1-12.

[18] Tungyshbayeva Z, Royer J.J., and Zhautikov T.M. 2015. *3D Modeling and Resources Estimation of a Gold Deposit, Zhungarie Province, Kazakhstan*. 13th Biennial SGA meeting, Nancy, France, 1-4.

[19] Uralkali 2013. *Sustainable Leadership*, Intregrated Report & Accounts 2013, 178p.

[20] USGS, Jan 2016, http://minerals.usgs.gov/minerals/pubs/commodity/potash/mcs-2015-potas.pdf

[21] USGS, 2009, http://minerals.usgs.gov/minerals/pubs/commodity/phosphate_rock/mcs-2009-phosp.pdf

[22] Wheeler, H. E. (1958) -Time-Stratigraphy. *Bulletin of the American Association of Petroleum Geologists*, **42**(5), 1047-1063.